manner. However, we believe this to be a rather conservative estimate, since the limiting factor should be in the refinement rather than solution, once a reliable starting model has been obtained. Indeed, Rudolf et al.[27] have recently solved the structure of an aluminophosphate molecular sieve containing 24 unique atoms, by direct methods.

The present example demonstrates the quality of refinement that may be obtained from synchrotron X-ray data for a pure, well-crystalline phase. The most impressive demonstration of this is the unconstrained refinement of the H atom position. The sensitivity of the refinement to the inclusion of the hydrogen atom probably stems from the fact that manganese occupies a special position and only contributes to 63 (hkl, $k + l = 2n$) out of a total of 135 reflections. For the remaining reflections the proportion of scattering due to hydrogen will be relatively high. However, our experience with other data sets suggests that in general major problems can arise in the refinement of X-ray data. Difficulties arise in adequately describing the X-ray peak shape, particularly when sample-related effects such as anisotropic particle size broadening become important. Future work will probably involve a combination of X-ray and neutron studies. X-ray diffraction is well suited to structure solution, particularly when heavy atoms are present, and neutron diffraction is more appropriate for refinement, due to the more predictable peak shapes.

Acknowledgment. A part of this research was carried out at the National Synchrotron Light Source, Brookhaven National Laboratory, which is supported by the Division of Materials Sciences and Division of Chemical Sciences, U.S. Department of Energy. In addition, we would like to thank D. E. Cox for experimental assistance and C. C. Torardi and J. B. Parise for assistance with local computer programs. P. L. would like to thank the SERC for provision of a Research Studentship and Du Pont for hospitality and support during a visit to the Experimental Station.

Registry No. $MnPO_4 \cdot H_2O$, 13446-43-0.

(27) Rudolf, P. R.; Saldarriaga-Molina, C.; Clearfield, A. *J. Phys. Chem.* **1986**, *90*, 6122.

Contribution from the Department of Hydrocarbon Chemistry and Division of Molecular Engineering, Faculty of Engineering, and Faculty of Pharmaceutical Sciences, Kyoto University, Kyoto 606, Japan

Structure and Oligomerization of Tetrakis(dithioheptanoato)diplatinum

Takashi Kawamura,*[1a,b] Tsuyoshi Ogawa,[1b] Tokio Yamabe,[1a,b] Hideki Masuda,[1c] and Tooru Taga*[1c]

Received March 27, 1987

The dinuclear complex $Pt_2(n\text{-}C_6H_{13}CS_2)_4$ has been prepared from K_2PtCl_4 and $n\text{-}C_6H_{13}CS_2H$. The crystal of the diplatinum complex is monoclinic, space group $C2/c$, with cell dimensions a = 36.043 (10) Å, b = 6.079 (1) Å, c = 17.910 (3) Å, β = 92.49 (2)°, and Z = 4. The structure consists of dinuclear units, with four bridging dithioheptanoato ligands, stacking on the crystallographic 2-fold axis with linear arrangement of Pt atoms. The intra- and intermolecular Pt–Pt distances are 2.855 and 3.224 Å, respectively. Its solution shows thermochromism (brown at room temperature and blue-green at lower temperatures) due to reversible dimerization and further oligomerization. The dimer shows a low-energy absorption at 460 nm, and further self-association induces an absorption at 595 nm, which is comparable with a 620-nm band in the reflectance spectrum of crystalline solids. Thermodynamic data of ΔH = −13 kcal/mol and ΔS = −41 cal/(mol K) have been obtained for the dimerization in toluene.

Introduction

Dinuclear complexes of Pt(II) such as $Pt_2(CH_3CS_2)_4$[2] and $K_4Pt_2(H_2P_2O_5)_4$[3] are of interest because of an intramolecular partial Pt(II)–Pt(II) bonding interaction arising from 5d–6p mixing[4] and because of the one-dimensional stack in the crystalline state. In the linear stack of $Pt_2(RCS_2)_4$ the intermolecular Pt–Pt distances are short enough (3.08–3.8 Å)[2,5] to produce unusual optical properties. The driving force to form their columnar structures has been suggested to originate from packing of the molecule in the crystalline space rather than intermolecular electronic metal–metal or metal–ligand interactions.[2]

The solubility of $Pt_2(CH_3CS_2)_4$ is not sufficient to investigate its properties in solution.[2] Tetrakis(dithio-2-methylpropanoato)diplatinum[5] has been reported to have some solubility in toluene, but its behavior in solution has not been explored. To investigate the molecular properties of this class of Pt(II)–Pt(II) d^8–d^8 systems, we have prepared tetrakis(dithioheptanoato)diplatinum, which has high solubility in organic solvents. The present paper reports the single-crystal X-ray determination of its structure and its reversible oligomerization in solution.

Experimental Section

Elemental analyses were performed by the Elemental Analysis Center, Kyoto University. Solvents were degassed by flushing with Ar for ca. 20 min when necessary. All reactions and measurements were carried out under Ar.

Spectroscopy. Electronic absorption spectra were recorded on a Hitachi 330 spectrophotometer. An Oxford DN1704 variable-temperature liquid-nitrogen cryostat was used to obtain spectra at temperatures below 0 °C. A Hitachi SPR-7 temperature controller was used to observe spectra at temperatures between 0 and 30 °C. Concentrations of solutions for measurements of electronic spectra were corrected for temperature-dependent volume changes by using the thermal expansion data of the pure solvent.[6] Reflectance spectra were observed by using a Hitachi U-3400 spectrophometer. Vibrational spectra were measured on a Nicolet 20DXB FTIR spectrometer. A Nicolet NT-300 NMR spectrometer was used to obtain ^1H NMR spectra.

Reagents. K_2PtCl_4, n-hexyl bromide, carbon disulfide, piperidine, and toluene-d_8 were obtained from Nakarai Chemicals. THF was distilled from sodium benzophenone ketyl under an Ar atmosphere prior to use. Toluene, n-hexane, and dichloromethane were distilled from calcium hydride before use.

Preparation of Piperidinium Dithioheptanoate.[7,8] To a mechanically stirred slurry solution of n-hexylmagnesium bromide prepared from 50 g (0.30 mol) of n-hexyl bromide and 7.3 g (0.30 mol) of magnesium turnings in 105 mL of THF cooled in an ice bath was added 22 g (0.30 mol) of carbon disulfide dropwise over 2.5 h, keeping the temperature of the reaction mixture below 8 °C. The mixture was stirred overnight in an ice bath. To this mixture was added dropwise 70 mL of ice-cold water flushed with Ar, and the mixture was acidified with dropwise addition of 100 mL of an ice-cold and degassed 6 mol L^{-1} HCl aqueous solution. After separation of the organic layer, the aqueous layer was extracted three times with 20 mL each of n-hexane and the hexane layer

(1) (a) Department of Hydrocarbon Chemistry. (b) Division of Molecular Engineering. (c) Faculty of Pharmaceutical Sciences.
(2) Bellito, C.; Flamini, A.; Piovesana, O.; Zanazzi, P. F. *Inorg. Chem.* **1980**, *19*, 3632.
(3) Filomena Dos Remedios Pinto, M. A.; Sadler, P. J.; Neidle, S.; Sanderson, M. R.; Subbiah, A.; Kuroda, R. *J. Chem. Soc., Chem. Commun.* **1980**, 13.
(4) Reis, A. H., Jr.; Peterson, S. W. *Inorg. Chem.* **1976**, *15*, 3186.
(5) Bellito, C.; Dessy, G.; Fares, V.; Flamini, A. *J. Chem. Soc., Chem. Commun.* **1981**, 409.
(6) Washburn, E. W., Ed. *International Critical Tables of Numerical Data, Physics, Chemistry and Technology*; NRC: Washington, DC, 1928; Vol. III.
(7) Cf.: Houben, J.; Schultze, K. M. L. *Ber. Dtsch. Chem. Ges.* **1910**, *43*, 2481.
(8) Cf.: Kato, S.; Mizuta, M. *Bull. Chem. Soc. Jpn.* **1972**, *45*, 3493.

0020-1669/87/1326-3547$01.50/0

was combined with the organic layer. The combined organic layer was carefully washed with water under Ar and dried over anhydrous magnesium sulfate. After evaporation of solvent, the residual brown oil was dissolved with 50 mL of ethyl acetate, 30 mL (0.30 mol) of piperidine was added, and the resulting solution was kept in a freezer overnight, giving piperidinium dithioheptanoate as orange-yellow plates, which were recrystallized from a mixture of *n*-hexane and dichloromethane, giving 7.2 g (0.29 mmol, 10% yield) of the pure salt. This crystalline salt can be handled under air but decomposed in 3 months even when kept under Ar in a refrigerator. IR (KBr pellet): 2943 (s), 2861 (s), 2738 (m), 2500 (m), 2361 (m), 1581 (m), 1450 (m), 1393 (w), 1261 (m), 1097 (s), 1023 (s), 941 (s), 859 (m), 802 (m), 671 (w), 539 (w), 433 (w) cm^{-1}. Anal. Calcd for $C_{12}H_{25}NS_2$: C, 58.23; H, 10.18; N, 5.66; S, 25.91. Found: C, 58.03; H, 10.28; N, 5.58; S, 25.91.

Preparation of Tetrakis(dithioheptanoato)diplatinum. Dithioheptanoic acid was liberated from 2.5 g (10 mmol) of piperidinium dithioheptanoate by treating the salt with 20 mL of a deoxygenated concentrated HCl aqueous solution and extracted three times with 10 mL each of *n*-hexane. The combined hexane layer was washed four times with 10 mL each of water and dried over anhydrous magnesium sulfate, and after filtration of the desiccant, the solvent was evaporated, leaving the acid as an orange oil. To the acid were added 36 mL of deoxygenated toluene and 0.70 g (1.7 mmol) of finely pulverized K_2PtCl_4, and the resulting mixture was refluxed for 85 h, during which the color of the reaction mixture changed from orange to dark brown. After filtration of the mixture, the filtrate was charged on a 32 × 300 mm column packed with Merck silica gel 60 and eluted with *n*-hexane, and the first reddish brown band was collected. Recrystallization from *n*-hexane gave 0.50 g (0.49 mmol, 57% yield based on K_2PtCl_4) of $Pt_2(n\text{-}C_6H_{13}CS_2)_4$ as needles with copper luster. Mp (in evacuated tube): 156–159 °C. IR (KBr pellet): 2959 (s), 2918 (s), 2845 (s), 1450 (s), 1417 (s), 1261 (m), 1204 (m), 1147 (s), 1040 (s), 1023 (m), 958 (s), 724 (m) cm^{-1}. ^1H NMR (300 MHz, toluene-d_8): δ 2.71 (t, J = 7.6 Hz), 1.76 (q, J = 7.4 Hz), 1.08–1.32 (m), 0.87 (t, J = 7.0 Hz). Anal. Calcd for $C_{28}H_{52}S_8Pt_2$: C, 32.47; H, 5.06; S, 22.77. Found: C, 32.73; H, 5.19; S, 22.67. This diplatinum complex was highly soluble in toluene and moderately soluble in hexane. In these solvents the complex was fairly stable under air. It had high solubility also in dichloromethane, chloroform, THF, and diethyl ether. The complex was practically insoluble in acetonitrile, DMSO, acetone, methanol, and water.

X-ray Structure Determination. Preliminary X-ray photographic examination established a monoclinic unit cell containing four chemical units of $Pt_2(n\text{-}C_6H_{13}CS_2)_4$. The systematic absences of hkl for $h + k = 2n + 1$ and $h0l$ for $l = 2n + 1$ led to two possible space groups of Cc and $C2/c$. A needlelike crystal of ca. 0.2 × 0.2 × 0.1 mm^3 with copper luster, grown from *n*-hexane solution, was mounted on a Rigaku AFC-5RU diffractometer that used a graphite-monochromated Cu Kα radiation ($\bar{\lambda}$ = 1.541 73 Å). The unit cell dimensions are a = 36.043 (10) Å, b = 6.079 (1) Å, and c = 17.910 (3) Å, and β = 92.49 (2)°. The formula weight is 1035.4 for $C_{28}H_{52}S_8Pt_2$; D_c = 1.754 g cm^{-3}.

Intensity data in the range $2\theta < 120°$ were collected at 25 °C in the ω–2θ scan mode with a ω scan rate of 8° min^{-1}. During the course of data collection, three reflections were monitored every 56 reflections. The intensity data were converted to F_o data in the usual manner. Absorption correction was applied in the cylindrical approximation (μR = 1.7). The standard deviations, $\sigma(F_o)$, were estimated by counting statistics. A total of 2419 independent reflections with $F_o \geq 3\sigma(F_o)$ were retained as observed and were used in solving and refining the structure.

The structure was solved by the heavy-atom method. The space group $C2/c$ was tentatively assumed, and successive Fourier syntheses revealed the approximate structure. It was refined with the block-diagonal least-squares method under each of the two possible space groups, C/c and $C2/c$, resulting in rejection of the former because this gave several wrong positional shifts from the normal bond distances and angles and nonpositive temperature factors for some light atoms. Several cycles of the refinement, including the anisotropic thermal parameters, were carried out to convergence with the weighting scheme $w^{-1} = (\sigma^2(F_o) + (0.023F_o)^2)$. Atomic scattering factors[9a] and anormalous dispersion terms[9b] were taken from ref 9. The hydrogen atoms were included as a fixed contribution in the last cycle; their positions were assumed to be in accord with the idealized geometry (C–H = 1.00 Å), and their temperature factors were assumed to be isotropic (B = 8.0Å^2). The final R and R_w values were 0.081 and 0.092, respectively. The final difference Fourier map showed no peaks greater than 0.75 e/Å^3, and none existed at chemically meaningful positions. All calculations were performed on a FACOM M382 computer at the Data Processing Center of Kyoto University by using the program system KPPXRAY.[10] The final positional and isotropic temperature factors of the non-hydrogen atoms are listed in Table I.

Table I. Fractional Atomic Coordinates[a] and Isotropic Equivalents of Thermal Parameters[b] for Non-Hydrogen Atoms of $Pt_2(n\text{-}C_6H_{13}CS_2)_4$

atom	x	y	z	B_{eq}, Å^2
Pt1	0.0	0.2944 (1)	0.2500	5.29
Pt2	0.0	−0.1753 (2)	0.2500	6.73
S1	0.0073 (1)	0.2984 (6)	0.3788 (2)	5.97
S2	−0.0639 (1)	0.3011 (8)	0.2618 (3)	8.38
S3	0.0351 (1)	−0.1795 (7)	0.3611 (2)	7.28
S4	−0.0525 (2)	−0.1800 (10)	0.3203 (3)	10.02
C1	0.0334 (4)	0.0754 (23)	0.3989 (8)	6.68
C2	0.0432 (5)	0.0873 (26)	0.4803 (9)	7.92
C3	0.0674 (4)	0.2837 (24)	0.4917 (10)	6.96
C4	0.1038 (6)	0.2678 (33)	0.4544 (11)	9.24
C5	0.1204 (5)	0.0395 (31)	0.4600 (12)	9.41
C6	0.1459 (5)	0.0091 (29)	0.3942 (9)	8.54
C7	0.1824 (5)	−0.1034 (31)	0.4239 (10)	9.89
C8	−0.0735 (4)	0.0692 (25)	0.3100 (8)	6.98
C9	−0.1139 (4)	0.0805 (25)	0.3208 (8)	7.03
C10	−0.1189 (4)	−0.1000 (25)	0.3772 (9)	7.07
C11	−0.1538 (5)	−0.2229 (31)	0.3522 (12)	9.17
C12	−0.1881 (6)	−0.0780 (34)	0.3418 (11)	10.25
C13	−0.2241 (6)	−0.2011 (31)	0.3186 (11)	9.17
C14	−0.2575 (5)	−0.0605 (30)	0.3074 (9)	11.86

[a] The esd's in parentheses refer to the last digit. [b] B_{eq} is the equivalent isotropic factor defined by Hamilton.[11]

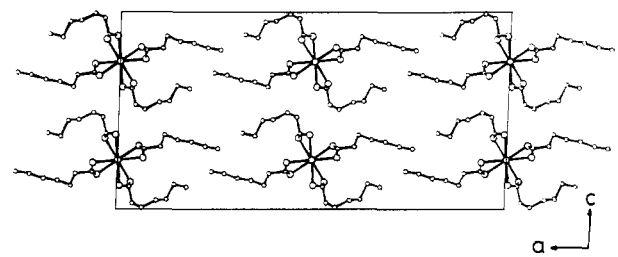

Figure 1. Crystal structure of $Pt_2(n\text{-}C_6H_{13}CS_2)_4$, projected along the crystallographic b axis.

Results and Discussion

Tetrakis(dithioheptanoato)diplatinum is obtained as needles with copper luster by reaction of K_2PtCl_4 and dithioheptanoic acid. This complex is stable under air in crystalline form and moderately stable in hydrocarbon solutions. It has high solubility toward hydrocarbons, haloalkanes, and ethereal solvents when compared with that of tetrakis(dithioacetato)diplatinum.[2]

Crystal Structure. The crystal structure of $Pt_2(n\text{-}C_6H_{13}CS_2)_4$ consists of linear stacks of dinuclear units that have four bridging dithioheptanoato ligands. The crystallographic 2-fold axis, which is parallel to the b axis, passes across the Pt–Pt axis. Figure 1 shows the crystal structure viewed down the b axis. A perspective drawing of a part of an infinite chain of the dinuclear unit is shown in Figure 2 together with the numbering of the atoms. Table II summarizes selected bond distances and angles around heavy atoms. The separation between Pt atoms of adjacent units is 3.224 Å. The intramolecular Pt–Pt distance is 2.855 Å, which is ca. 0.06 Å shorter than the distance between the mean planes defined by the four sulfur atoms. The two PtS_4 planes are twisted by ca. 27° from the eclipsed D_{4h} arrangement. For the dithioheptanoato ligand, the average S–C bond length and the average S–C–S bond angle are 1.69 Å and 133°, respectively. Interatomic distances and angles of $Pt_2(n\text{-}C_6H_{13}CS_2)_4$ are compared with those of $Pt_2(CH_3CS_2)_4$,[2] and $Pt_2(i\text{-}C_3H_7CS_2)_4$[5] in Table III.

Electronic Spectra. Electronic spectral data of $Pt_2(n\text{-}C_6H_{13}CS_2)_4$ are tabulated in Table IV together with those of

(9) Ibers, J. A., Hamilton, W. C., Ed. *International Tables for X-Ray Crystallography*; Kynoch: Birmingham, England, 1974; Vol. IV: (a) p 99; (b) p 148.

(10) Taga, T.; Higashi, T.; Iizuka, H. *KPPXRAY, Kyoto Program Package for X-ray Crystal Structure Analysis*; Kyoto University: Kyoto, Japan, 1985.

(11) Hamilton, W. C. *Acta Crystallogr.* **1959**, *12*, 609.

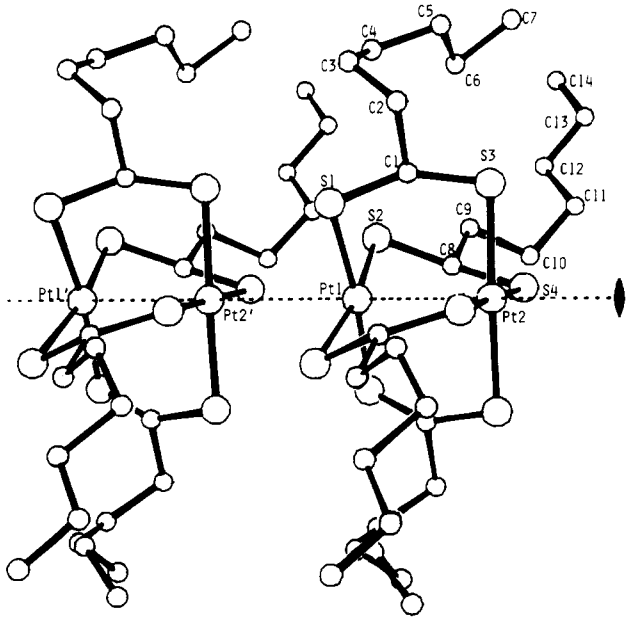

Figure 2. Molecular structure of $Pt_2(n\text{-}C_6H_{13}CS_2)_4$. The dotted line shows the crystallographic 2-fold axis.

Table II. Selected Interatomic Distances (Å) and Angles (deg) for $Pt_2(n\text{-}C_6H_{13}CS_2)_4$

	(1) Interatomic Distances		
Pt1–Pt2	2.855 (1)	Pt1–Pt2'[a]	3.224 (1)
Pt1–S2	2.322 (4)	Pt1–S1	2.311 (4)
Pt2–S4	2.318 (7)	Pt2–S3	2.311 (4)
S2–C8	1.697 (16)	S1–C1	1.680 (14)
S4–C8	1.700 (16)	S3–C1	1.693 (15)
	(2) Bond Angles		
Pt2–Pt1–S1	90.6 (1)	Pt2–Pt1–S2	91.0 (1)
S1–Pt1–S2	91.2 (2)	Pt1–Pt2–S3	90.6 (1)
Pt1–Pt2–S4	90.7 (2)	S3–Pt2–S4	92.2 (2)
Pt1–S1–C1	104.1 (5)	Pt1–S2–C8	104.9 (5)
Pt2–S3–C1	107.8 (5)	Pt2–S4–C8	107.5 (6)
S1–C1–S3	133.0 (9)	S2–C8–S4	134.1 (10)

[a] Intermolecular Pt–Pt distance.

$Pt_2(CH_3CS_2)_4$. The data of the solution spectrum has been obtained at the concentration of 0.04 mmol L^{-1} at room temperature where the fraction of the complex existing as oligomers is negligibly small (ca. 2×10^{-4}, vide supra). The solution spectrum of $Pt_2(n\text{-}C_6H_{13}CS_2)_4$ is similar to that of $Pt_2(CH_3CS_2)_4$. In the reflectance spectrum, $Pt_2(n\text{-}C_6H_{13}CS_2)_4$ gives only one low-energy band (16.3×10^3 cm^{-1}) below the transition energies in the solution spectrum, whereas two low-energy bands have been observed in that of $Pt_2(CH_3CS_2)_4$. These low-energy bands should be arising from electronic interactions between dinuclear units in the linear stack in the crystalline states.

The color of toluene, CH_2Cl_2, or THF solution of $Pt_2(n\text{-}C_6H_{13}CS_2)_4$ changes reversibly upon changes of the temperature. It is brown at room temperature and is blue-green at lower temperatures. Figure 3 shows the temperature dependence of 0.5 mmol L^{-1} solution of the complex in toluene as well as the diffuse reflectance spectrum of the powdered crystalline complex diluted with MgO.

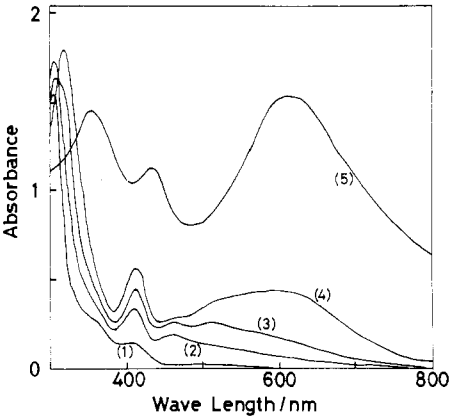

Figure 3. Electronic spectra of $Pt_2(n\text{-}C_6H_{13}CS_2)_4$. Absorption spectra of a 0.5 mmol L^{-1} toluene solution in a 1-mm path length cell observed at (1) 23, (2) −40, (3) −70, and (4) −90 °C, and (5) a diffuse reflectance spectrum (in arbitrary unit) of a powdered crystalline sample diluted with MgO observed at room temperature.

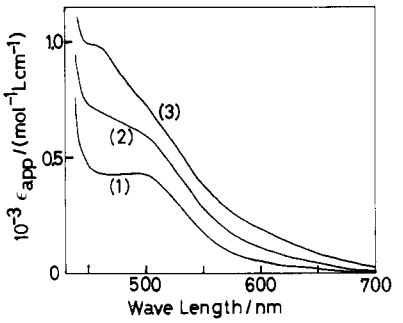

Figure 4. Electronic spectra of $Pt_2(n\text{-}C_6H_{13}CS_2)_4$ in toluene at −10 °C: (1) 0.2, (2) 0.5, and (3) 1 mmol L^{-1}.

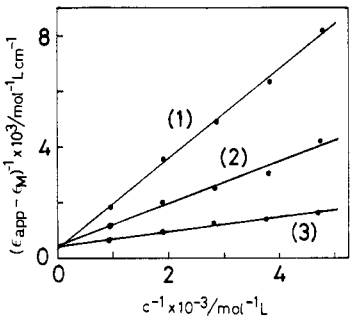

Figure 5. Plot of $(\epsilon_{app}-\epsilon_M)^{-1}$ vs c^{-1} at (1) −10, (2) −20, and (3) −30 °C.

Equilibrium between Monomer and Dimer. Since the temperature dependence of absorption spectra of solutions of the diplatinum complex is indicative of reversible dimerization of the dinuclear complex and of further oligomerization at lower temperatures, the concentration dependence of the spectra of toluene solutions were examined to see the monomer–dimer equilibrium. Figure 4 shows representative low-energy absorptions of dilute

Table III. Distances (Å) and Angles (deg) in $Pt_2(RCS_2)_4$

R	Pt–Pt intramol[a]	Pt–Pt intermol[b]	incline[c]	Pt–S	∠PtPtS	S–C	∠SCS
CH_3[d]	2.767	3.819 3.776	28	2.317	92.1	1.68	129.5
i-Pr[e]	2.795	3.081	0	2.31	*f*	1.71	*f*
i-Pr[g]	2.85	3.40	*f*	*f*	*f*	*f*	*f*
$n\text{-}C_6H_{13}$[h]	2.855	3.224	0	2.32	90.7	1.69	133

[a] Intramolecular distance. [b] Intermolecular distance. [c] Incline of the intramolecular Pt–Pt axis from the axis of the linear stack. [d] Reference 2. [e] For the deep purple crystal (form A) in ref 5. [f] Not reported. [g] Preliminary results for the green crystal (form B) in ref 5. [h] Present work.

Table IV. Electronic Spectra of $Pt_2(n\text{-}C_6H_{13}CS_2)_4$ and $Pt_2(CH_3CS_2)_4$[a]

$Pt_2(n\text{-}C_6H_{13}CS_2)_4$[b]		$Pt_2(CH_3CS_2)_4$[c]	
soln[d]	refl[e]	soln	refl
	16.3		15.2
			19.0
20.2 (2.55)	23.0	22.8 (~2.9) sh	22.7
24.8 (3.43)		24.6 (3.10)	24.4
28.6 (4.07) sh	28.4	28.9 (~3.2) sh	*f*
32.6 (4.47)	*g*	32.8 (4.20)	
g		~34.5 (~4.1) sh	
		~37.7 (~4.0) sh	

[a] Energies in 10^3 cm^{-1} (log ϵ in parentheses). sh = shoulder. [b] Present work. [c] Reference 2. [d] A 0.04 mmol/L solution in toluene at room temperature. [e] Reflectance spectrum. [f] Not reported beyond this frequency. [g] Not measured beyond this frequency.

solutions of the dinuclear complex at −10 °C. An increase in the concentration induces an enhanced increase of the apparent absorption coefficient, ϵ_{app}, at 460 nm.

When there exists an equilibrium between monomer and dimer

$$2\text{“}Pt_2\text{”} \overset{K}{\rightleftharpoons} (\text{“}Pt_2\text{”})_2 \qquad (1)$$

the following relation is expected between ϵ_{app} and the total concentration of the dinuclear unit, c, when the fraction of the dinuclear units existing as the dimer is small in comparison to unity:

$$(\epsilon_{app} - \epsilon_M)^{-1} = (\epsilon_D - 2\epsilon_M)^{-1}K^{-1}c^{-1} + 4(\epsilon_D - 2\epsilon_M)^{-1} \qquad (2)$$

Here, ϵ_M and ϵ_D are absorption coefficients for the monomer and the dimer, respectively. The value of ϵ_M at 460 nm has been obtained as 330 mol^{-1} L cm^{-1} from spectra of dilute (less than 0.1 mmol L^{-1}) solutions at room temperature and used as a temperature-independent constant[12] throughout the analysis. The spectra observed at −10, −20, and −30 °C with concentrations ranging from 0.2 to 1 mmol L^{-1} give plots of $(\epsilon_{app} - \epsilon_M)^{-1}$ vs c^{-1} as shown in Figure 5. The plots form straight lines with a common intercept in accordance with eq 2, $4(\epsilon_D - 2\epsilon_M)^{-1}$, identifying the absorption peak at 460 nm as due to the dimer.[13] The intercept corresponds to $\epsilon_D = 1.09 \times 10^4$ mol^{-1} L cm^{-1} (±10%) for the 460-nm peak. The slopes give values of the equilibrium constant, K, of 51.2, 151, and 389 mol^{-1} L for −10, −20, and −30 °C, respectively, which correspond to $\Delta H = -13$ kcal mol^{-1} and $\Delta S = -41$ cal K^{-1} mol^{-1} for the formation of the dimer.

When the temperature is lowered, new low-energy bands are developed at 510 and 595 nm as shown in Figure 3, indicating that further oligomerization takes place. The resemblance of the 595-nm band in the solution spectrum to the 620-nm band in the solid-state spectrum suggests that the oligomer in the solution has a linear chain of Pt atoms as in the crystalline state.

Intra- and Intermolecular Pt–Pt Interactions. The intramolecular Pt–Pt distances of diplatinum dithiocarboxylates in Table III are comparable with Pt(II)–Pt(II) distances in $[Pt_2(HO(O)POP(O)OH)_4]^{4-}$ (2.925 Å)[3] and the head-to-tail and head-to-head isomers of $[Pt_2(NH_3)_4(C_5H_4N)_4]^{2+}$ (2.90 and 2.88 Å, respectively).[14]

Intramolecular Pt–Pt distances in $Pt_2(CH_3CS_2)_4$ and $Pt_2(n\text{-}C_6H_{13}CS_2)_4$ are 0.17 and 0.06 Å shorter than distances between the mean planes defined by the four sulfur atoms, respectively, suggesting the existence of direct electronic bonding interactions between the Pt atoms. Among the diplatinum complexes in Table III, both the deep purple crystal of $Pt_2(i\text{-}PrCS_2)_4$ (designated as form A in ref 5) and the crystal of $Pt_2(n\text{-}C_6H_{13}CS_2)_4$ have exactly linear Pt chains. The former, which has a shorter intramolecular Pt–Pt distance than the latter, has also a shorter intermolecular Pt–Pt distance. This is contrary to a primitive expectation that a shorter intramolecular Pt–Pt distance would be accompanied with a longer intermolecular one as in most cases of trans effects.

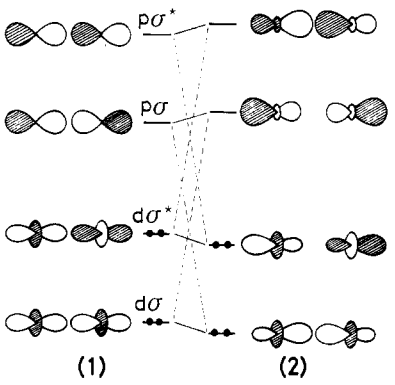

Figure 6. Pt–Pt σ MO's (1) before and (2) after 5d–6p mixing.

The dominant intramolecular Pt–Pt bonding interaction would arise from valence-shell d–p mixing in Pt–Pt σ-type orbitals[4,15,16] as has been proposed for d^8–d^8 metal–metal bonding in $[Pt_2(\mu\text{-}HO(O)POP(O)OH)_4]^{4-}$[17,18] and in $[Rh(RNC)_4]_2^{2+}$.[19,20] Admixture of the vacant Pt–Pt pσ or pσ* orbital into the occupied Pt–Pt dσ or dσ* orbital should take place in a phase to convert the occupied bonding and antibonding orbitals part way into still more bonding and nonbonding ones, respectively (Figure 6).[21-23] These deformations result in net bonding effects between the intramolecular pair of Pt atoms, which has a "formal bond order" of zero.

This p–d mixing results in expansion of lobes of both high-lying occupied dσ* and low-lying vacant pσ orbitals outward from the intramolecular Pt–Pt bonding region as shown in Figure 6. This expansion is favorable to intermolecular metal–metal interactions. In the dimer or oligomer, electrons in the high-lying dσ* orbital should be delocalized into the low-lying vacant pσ of the adjacent unit, resulting in intermolecular bonding effects. We suggest this to be a major driving force for the self-association. This delocalization, which results in decrease and increase of electron populations in the dσ* and pσ orbitals, respectively, should induce a decrease of the intramolecular Pt–Pt distance. Thus the present bonding model suggests that a short intermolecular Pt–Pt distance would induce decrease of the intramolecular Pt–Pt distance if all other factors are same. This is parallel to the present observation.

Acknowledgment. We thank Professor S. Kato (Gifu University) for helpful suggestions for the preparation and purification of dithioheptanoic acid. We are indebted to Mr. Komori (Hitachi) for the measurements of the reflectance spectra.

Supplementary Material Available: Tables listing bond lengths and valence angles (Table SI), torsion angles (Table SII), fractional coordinates for hydrogen atoms (Table SIII), and anisotropic thermal parameters for non-hydrogen atoms (Table SIV) (3 pages); a table of calculated and observed structure factors (11 pages). Ordering information is given on any current masthead page.

(12) The temperature dependence of the absorbance at 460 nm of a 40 μmol L^{-1} solution of the diplatinum complex in toluene was less than experimental errors (±5%) between 0 and 30 °C, where the fraction of the dinuclear unit existing as the dimer is estimated to be less than 2×10^{-3} (vide supra). By extrapolation of this observation, ϵ_M at 460 nm has been assumed to be temperature independent between −10 and −30 °C.
(13) This does not necessarily mean that ϵ_D at 460 nm is temperature independent but means that its temperature dependence is less than the errors in the plots in Figure 5.
(14) Hollis, L. S.; Lippard, S. J. *J. Am. Chem. Soc.* **1981**, *103*, 1230.
(15) Isci, H.; Mason, W. R. *Inorg. Chem.* **1975**, *13*, 1175.
(16) Ciullo, G.; Piovesana, O. *Inorg. Chem.* **1980**, *19*, 2871.
(17) Fordyce, W. A.; Brummer, J. G.; Crosby, G. A. *J. Am. Chem., Soc.* **1981**, *103*, 7061.
(18) Rice, S. F.; Gray, H. B. *J. Am. Chem. Soc.* **1983**, *105*, 4571.
(19) Mann, K. R.; Gordon, J. G., II; Gray, H. B. *J. Am. Chem. Soc.* **1975**, *97*, 3553.
(20) Lewis, N. S.; Mann, K. R.; Gordon, J. G., II; Gray, H. B. *J. Am. Chem. Soc.* **1976**, *98*, 7461.
(21) (a) Dedieu, A.; Hoffmann, R. *J. Am. Chem. Soc.* **1978**, *100*, 2078. (b) Mehrota, P. K.; Hoffmann, R. *Inorg. Chem.* **1978**, *17*, 2187.
(22) Christoph, G. G.; Koh, Y.-B. *J. Am. Chem. Soc.* **1979**, *101*, 1422.
(23) Sowa, T.; Kawamura, T.; Yamabe, T.; Yonezawa, T. *J. Am. Chem. Soc.* **1985**, *107*, 6471.